Chapter 4

Precipitation Synthesis as a Route to Lanthanide Hydroxynitrate Anion Exchange Materials and Layered Hydroxides Containing Precious Metals

4.0 Introduction

The synthesis of the first anion exchange intercalation hosts to combine the properties of the smaller lanthanide cations with the flexibility of intercalation compounds were discussed in detail in Chapter 2. These materials, $Ln_2(OH)_5NO_3{\cdot}1.5H_2O$ (Ln = Y, Gd–Lu), are synthesised hydrothermally and have an interlayer separation of approximately 9.1 Å. They were found to undergo facile anion exchange reactions at room temperature with a range of organic carboxylate and sulfonate salts. The synthesis, structures and anion exchange properties of the analogous chloride phases, $Ln_2(OH)_5Cl{\cdot}nH_2O$ (Ln = Y, Nd–Yb) were also discussed. Both families show a variation in hydration levels, which as the water molecules are bound to the lanthanide cations, leads to subtle differences in the layer structure which is comprised of 8- and 9-coordinate Ln^{3+} sites. In the case of the $Yb_2(OH)_5X{\cdot}1.5H_2O$ (X = NO_3, Cl) material polymorphism has been observed with both orthorhombic and monoclinic structures accessible.

Materials of similar compositions, prepared by homogeneous precipitation have subsequently been reported in the literature. $Ln_8(OH)_{20}Cl_4{\cdot}nH_2O$ (Ln = Nd, Sm-Tm, and Y; $n \approx 6$ - 7) are synthesised by refluxing $LnCl_3{\cdot}xH_2O$, NaCl and HMT (hexamethylenetetramine) in water, under nitrogen for a period of 10 - 12 hours.[1, 2] It was noted that the materials were highly sensitive to humidity levels, with Sm, Eu and Gd samples exhibiting reversible layer expansion and contraction behaviour according to hydration levels.

Owing to the affects of varying levels of hydration on materials of this type it was deemed to be of interest to further explore possible compositions of layered hydroxynitrate materials. An additional possibility is to expand the series to include $Ln(OH)_2(NO_3)\cdot xH_2O$ with preparation methods, particularly coprecipitation, for layered hydroxy nitrates already present in the literature.

In the pursuit of novel layered hydroxides incorporating metals with interesting properties including optical and catalytic, attention was turned to Ru and Pd. Commonly, in order to achieve a high surface area and improved thermal stability, catalysts are dispersed on a porous support through liquid-phase impregnation. The problems incurred as a result of this method have been reviewed by Komiyama; these include non-uniform distribution of catalyst particles.[3] It is envisaged that layered hydroxide materials incorporating Ru and Pd with uniform metal cation distribution would be highly active catalysts and thus be suitable for industrial applications.

A review of the literature reveals that the photoactive complex anion $Ru(BPS)_3^{4-}$ (BPS = 4,7-diphenyl-1,10-phenanthrolinedisulfonate) has been incorporated between the layers of MgAl-LDH by a coprecipitation method.[4] $[RuCl_5H_2O]^{2-}$ has been intercalated into ZnAl-LDH by anion exchange.[5] MgAl LDH has also been used as a support for $RuCl_3$, and functions as an efficient catalyst in the oxidation of 1,2-dihaloalkenes.[6]

A number of works have attempted to synthesise new layered hydroxides containing noble metals, with the aim of producing new catalysts and catalyst precursors.
Kaneda has demonstrated the synthesis of ruthenium-containing MgAl-LDHs, obtaining $Mg_6Al_2Ru_{0.5}(OH)_{16}CO_3$ from a coprecipitation route.[7] The utility of the material as a heterogeneous catalyst in the oxidation of allylic and benzylic alcohols in the presence of atmospheric oxygen was demonstrated. In a representative reaction with cinnamyl alcohol, a 73 % conversion was achieved in 5 hours to give a cinnamaldehyde yield of 68 %.[8] Improved catalytic activity in this reaction is achieved by ruthenium-containing MAl-LDHs (M = Mn, Fe, Zn, Mg and Co).[9] Here, RuCo-LDH (Ru:Co:Al ratio 0.3:3:1) is cited as the most efficient catalyst with 100 % conversion for cinnamyl alchohol in 40 minutes by GC, giving an 89 % isolated

yield of cinnamaldehyde. In both cases the LDH is easily removed from the reaction mixture and shows no appreciable loss of activity upon recycling.

Rh and Ru containing MgAl LDHs have been synthesised as catalyst precursors for use in the partial oxidation of methane.[10, 11] Ru doping levels of 1 and 5 % into the MgAl LDH was achieved, upon calcination at 1173 K. However, a significant amount of RuO_2 was formed, thus a lower catalytic activity was observed compared with the Rh containing sample.

Basile *et al.* have further sought to expand the range of precious metals incorporated into MgAl LDH materials to include Ir, Pd and Pt.[12] The amount of metal incorporated varied between 0.04 % to 5 % with a loss of Pt of around 20 % relative to the starting material. Calcination at 923 K allowed the derivation of a scale of stability of the order Rh > Ir > Ru > Pd > Pt.

4.1 Scope of Chapter

The first part of this chapter concerns the room temperature precipitation synthesis of layered lanthanide hydroxynitrate intercalation hosts ($Ln_2(OH)_5NO_3{\cdot}H_2O$, Ln = Y, Eu, Tb, Ho) including the first $Eu_2(OH)_5NO_3{\cdot}H_2O$ host lattice. The materials are characterised and anion exchange reactions with a range of organic carboxylates and sulfates are investigated.

Further, the feasibility of incorporating precious metals Ru and Pd into layered hydroxides is considered. A number of methods are examined, namely hydrothermal synthesis, coprecipitation and vapour diffusion. The results of these experiments are presented and preliminary conclusions are drawn.

4.2 Precipitation Synthesis of Lanthanide Hydroxynitrate Anion Exchange Materials, $Ln_2(OH)_5NO_3{\cdot}H_2O$ (Ln = Y, Eu-Er)

4.2.1 Results and Discussion

A room temperature precipitation method has been used to synthesise a new family of anion exchange intercalation hosts. In a typical experiment, NaOH was added dropwise on to solid $Ln(NO_3)_3{\cdot}xH_2O$ (Ln = Y, La–Lu) and stirred at room temperature, the resulting solid was filtered, washed and dried in air.

The composition of the host lattices has been confirmed by TGA and elemental analysis as $Ln_2(OH)_5NO_3{\cdot}H_2O$ (Ln = Y, Eu-Er). Characterising data for the materials is summarised below.

Table 1 Characterising data for the layered lanthanide hydroxynitrate phases, $Ln_2(OH)_5NO_3{\cdot}H_2O$ (Ln = Y, Eu, Tb, Ho).

Ln	Composition	Interlayer Separation (Å)	Elemental Analysis	
			Observed (%)	Calculated (%)
Y	$Y_2(OH)_5(NO_3)_{0.90}(CO_3)_{0.05}{\cdot}H_2O$	8.45	N (3.60) H (1.91) C (1.35)	N (3.71) H (2.08) C (0.18)
Eu	$Eu_2(OH)_5(NO_3)_{0.70}(CO_3)_{0.15}{\cdot}H_2O$	8.41	N (2.31) H (1.44) C (0.25)	N (2.22) H (1.14) C (0.41)
Tb	$Tb_2(OH)_5(NO_3)_{0.78}(CO_3)_{0.11}{\cdot}H_2O$	8.43	N (2.21) H (1.33) C (0.38)	N (2.29) H (1.48) C (0.27)
Ho	$Ho_2(OH)_5(NO_3)_{0.74}(CO_3)_{0.13}{\cdot}H_2O$	8.51	N (1.99) H (1.30) C (0.49)	N (2.13) H (1.45) C (0.32)

A small amount of carbonate contamination is present in these materials, as is common in layered hydroxides prepared via a precipitation route where atmospheric carbon dioxide is absorbed to generate carbonate anions *in situ*. This has been encountered in the synthesis of LDHs[13-15] as well as the lanthanide phases reported by Geng *et al.* for the $Ln_8(OH)_{20}Cl_4{\cdot}nH_2O$ (Ln = Y, Nd, Sm -Tm) materials.[1]

As the materials are isostructural and display similar anion exchange behaviour, discussion of the phases in this chapter will be limited to $Y_2(OH)_5(NO_3)_{0.90}(CO_3)_{0.05}{\cdot}H_2O$.

The TGA data for $Y_2(OH)_5(NO_3)_{0.90}(CO_3)_{0.05}{\cdot}H_2O$ is shown in Figure 1 and displays three distinct mass losses comparable to those seen for other layered hydroxides. The first mass loss of 5.9 % (calculated value is 5.3 %) below 170 ºC corresponds to the loss of co-intercalated water. The second mass loss of 10.8 % (10.6 %) by 350 ºC corresponds to partial decomposition of the layers leaving a material of nominal composition '$Y_2O_2(OH)(NO_3)_{0.90}(CO_3)_{0.05}$'.[16] By 650 ºC final decomposition to Y_2O_3 is complete with a mass loss of 18.6 % (17.6 %). No further mass loss is observed above 700 ºC.

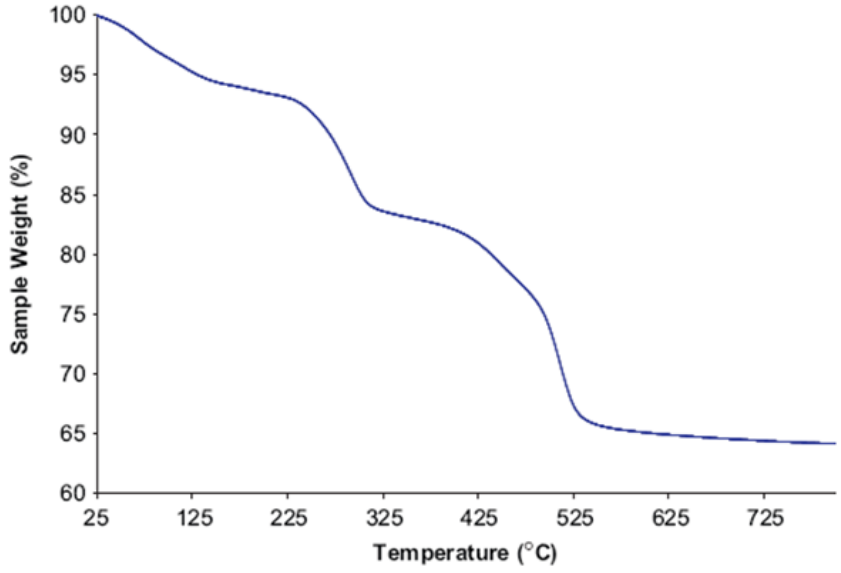

Figure 1 TGA trace for $Y_2(OH)_5(NO_3)_{0.90}(CO_3)_{0.05}{\cdot}H_2O$ showing mass losses of 5.9 % below 170 ºC and further mass losses of 10.8 % by 350 ºC and 18.6 % by 700 ºC.

As may be expected, these materials are of reduced crystallinity compared with those prepared by hydrothermal synthesis (as discussed in Chapter 2). Powder X-ray diffraction data shown in Figure 2 displays 00*l* reflections characteristic of lamellar phases, less apparent are the non-(00*l*) reflections indicative of ordering within the layers. The interlayer separation for this phase is 8.45 Å, markedly reduced from the related $Y_2(OH)_5NO_3{\cdot}1.5H_2O$ phase (d = 9.18 Å) as a consequence of reduced hydration level.

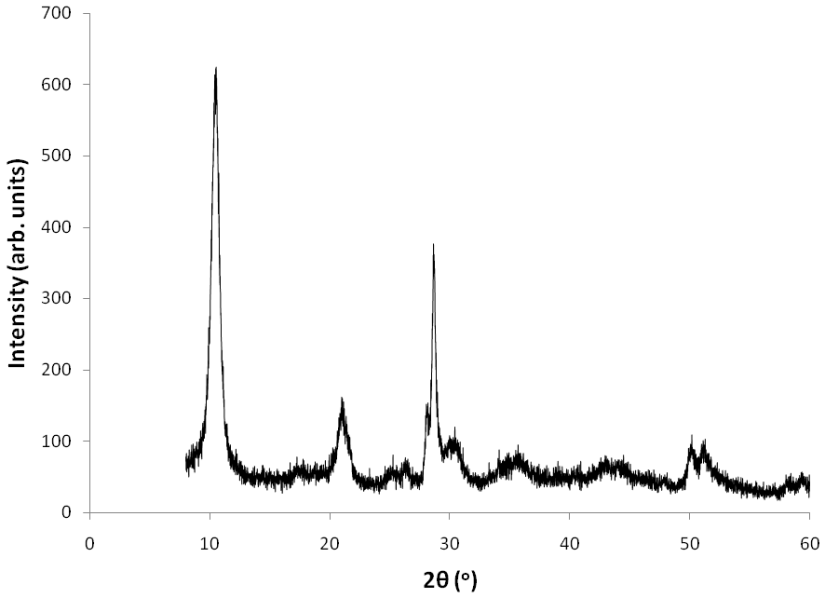

Figure 2 Powder X-ray diffraction pattern of $Y_2(OH)_5(NO_3)_{0.90}(CO_3)_{0.05}{\cdot}H_2O$.

Indexing of the unit cell for these materials has been precluded by their poorly crystalline nature and the insufficient number of non-(00*l*) reflections observed in PXRD data. Previous reports in the literature suggest an orthorhombic cell for $Ln_2(OH)_5NO_3{\cdot}2H_2O$ Ln = Y and Yb materials, with unit cell parameters *a* = 6.040(4) Å, *b* = 3.800(1) Å, *c* = 8.533(3) Å and *a* = 5.964(2) Å, *b* = 3.750(1) Å, *c* = 8.526(3) Å respectively.[17] Attempts to index the reflections for these materials with the unit cell parameters given have proved unsuccessful. Though the d-spacing given for the $Yb_2(OH)_5NO_3{\cdot}2H_2O$ is similar (8.51 Å) the hydration level for these phases differs from those described here. Examination of the powder X-ray diffraction patterns for the $Ln_2(OH)_5NO_3{\cdot}H_2O$ materials did not suggest the presence of any other known phases.

$Yb_2(OH)_5NO_3{\cdot}H_2O$ is very poorly crystalline, as is evidenced in the XRD pattern shown in Figure 3a. This observation strongly contrasts with that of the crystalline $Yb_2(OH)_5NO_3{\cdot}1.5H_2O$ phase, indicating the significance of hydration levels in the morphology of these materials. The importance of synthetic method is underlined by the formation of phase pure microcrystalline $Yb_2(OH)_5Cl{\cdot}1.5H_2O$ (including single crystals) under hydrothermal conditions where synthesis via precipitation under reflux did not proceed.[1] As for the $Ln_2(OH)_5NO_3{\cdot}1.5H_2O$ materials, there is also a limiting cation size for the $Ln_2(OH)_5NO_3{\cdot}H_2O$ phase, evidenced by unsuccessful attempts to synthesise the Tm and Lu analogues (Figure 3b-c). The larger lanthanides, all formed poorly crystalline material except $La(OH)_2NO_3$ in the case of lanthanum.

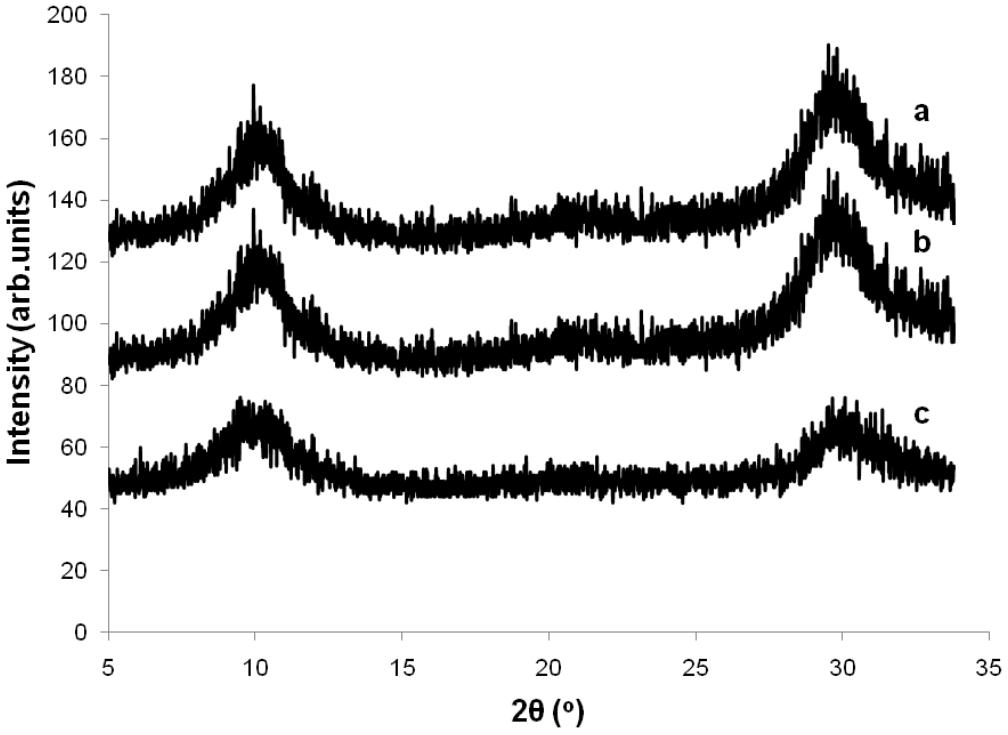

Figure 3 Powder X-ray diffraction pattern for the attempted synthesis of:

(a) $Yb_2(OH)_5NO_3{\cdot}H_2O$,

(b) $Tm_2(OH)_5NO_3{\cdot}H_2O$,

(c) $Lu_2(OH)_5NO_3{\cdot}H_2O$.

Synthesis of the Dy material proved unsuccessful, yielding poorly crystalline material (Figure 4a). The Er material was not prepared phase pure, with the sample containing significant amounts of $Er(OH)_3$.[18]

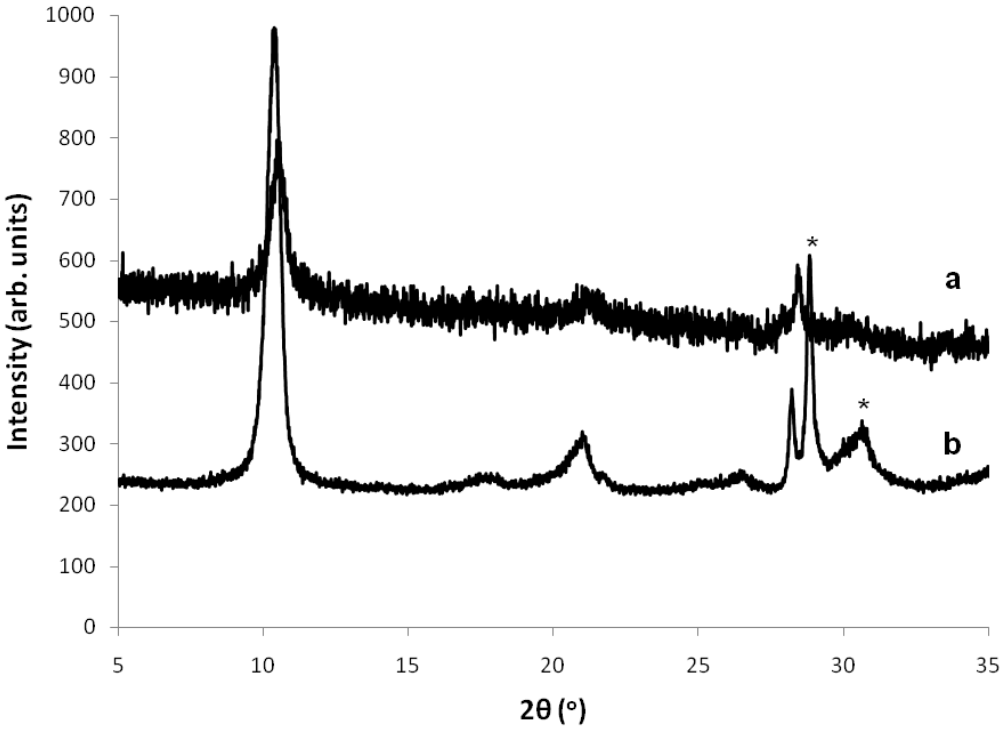

Figure 4 Powder X-ray diffraction pattern for the attempted synthesis of:

(a) $Dy_2(OH)_5NO_3{\cdot}H_2O$,

(b) $Er_2(OH)_5NO_3{\cdot}H_2O$ (* indicates presence of $Er(OH)_3$).

The FTIR spectrum of $Y_2(OH)_5NO_3{\cdot}H_2O$ is shown in Figure 5. The key features in the spectrum are a broad absorption band at approximately 3500 cm^{-1} corresponding to a combination of the stretching vibrations of the layer hydroxyl groups and the interlayer water molecules. The bending vibration of the water molecules is visible at 1640 cm^{-1}. The broad band at approximately 1370 cm^{-1} is in agreement with the presence of an uncoordinated nitrate anion located between the layers. This is comparable to observations made on other layered hydroxides containing interlayer nitrate groups.[15, 19] This is further evidenced by bands at approximately 1050 cm^{-1} (ν_1 mode resulting from reduced symmetry of the intercalate) and 1760 cm^{-1} (combination mode typical of nitrate) and these are of increased importance given the carbonate contamination of the phase, for which the ν_3 mode also appears in the region 1340 – 1400 cm^{-1}.

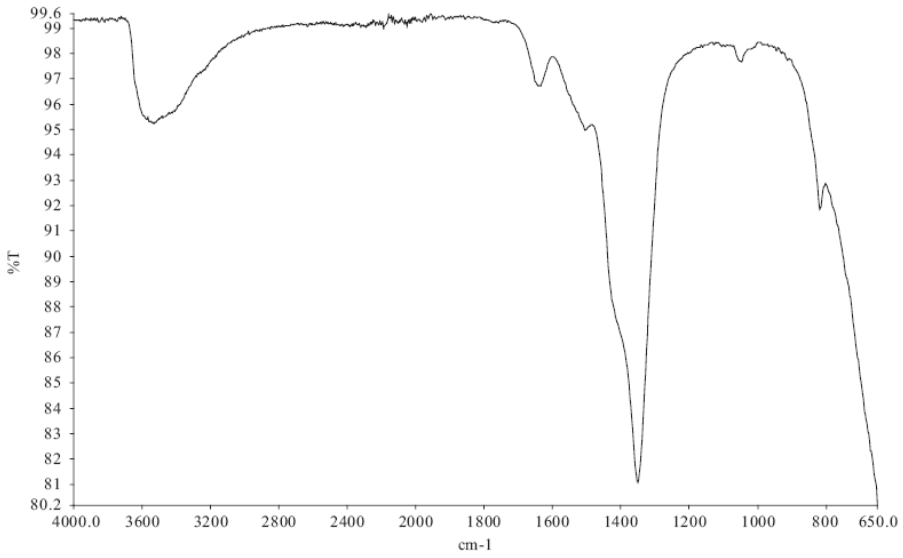

Figure 5 FTIR spectrum for $Y_2(OH)_5NO_3{\cdot}H_2O$.

4.2.2 Anion Exchange

Anion exchange reactions were carried out with a range of organic carboxylate and sulfonate anions, and these proved successful at room temperature. Complete exchange was verified by the absence of reflections characteristic of the host lattice in the powder X-ray diffraction patterns of the intercalates and of nitrogen in

elemental analysis. Reactions to give $Y_2(OH)_5A_{0.5}\cdot H_2O$ proceeded where A = terephthalate, fumarate, malonate, succinate, decyl sulphate and 2,6-naphthalene disulfonate, however reaction with the maleate anion proved to be incomplete. The characterising data for the anion exchange derivatives of $Y_2(OH)_5NO_3\cdot H_2O$ is summarized in

Table **2** and typical powder X-ray diffraction patterns for the materials are shown in Figure 6.

Table 2 Characterising data for the organic anion exchange derivatives of $Y_2(OH)_5NO_3\cdot H_2O$

Anion	Composition	Interlayer Separation (Å)	Elemental Analysis	
			Observed (%)	Calculated (%)
Malonate†	$Y_2(OH)_5(C_3H_2O_4)_{0.5}\cdot H_2O$	10.83	C (5.93)	C (5.42)
			H (2.51)	H (2.43)
Fumarate†	$Y_2(OH)_5(trans\text{-}C_4H_2O_4)_{0.5}\cdot H_2O$	10.78	C (7.58)	C (7.11)
			H (2.65)	H (2.39)
Terephthalate†	$Y_2(OH)_5(p\text{-}C_8H_4O_4)_{0.5}\cdot H_2O$	12.84	C (13.66)	C (13.24)
			H (2.67)	H (2.50)
Succinate†	$Y_2(OH)_5(C_4H_4O_4)_{0.5}\cdot H_2O$	11.30	C (7.59)	C (7.09)
			H (2.75)	H (2.68)
Decylsulfonate	$Y_2(OH)_5(C_{10}H_{21}SO_4)\cdot 3H_2O$	24.30	C (20.88)	C (22.31)
			H (5.26)	H (5.99)
2,6-NDS†	$Y_2(OH)_5(C_{10}H_6(SO_3)_2)_{0.5}\cdot 3H_2O$	15.45	C (12.72)	C (13.05)
			H (2.64)	H (3.06)

† Reactions carried out by Miss S. A. Hindocha.

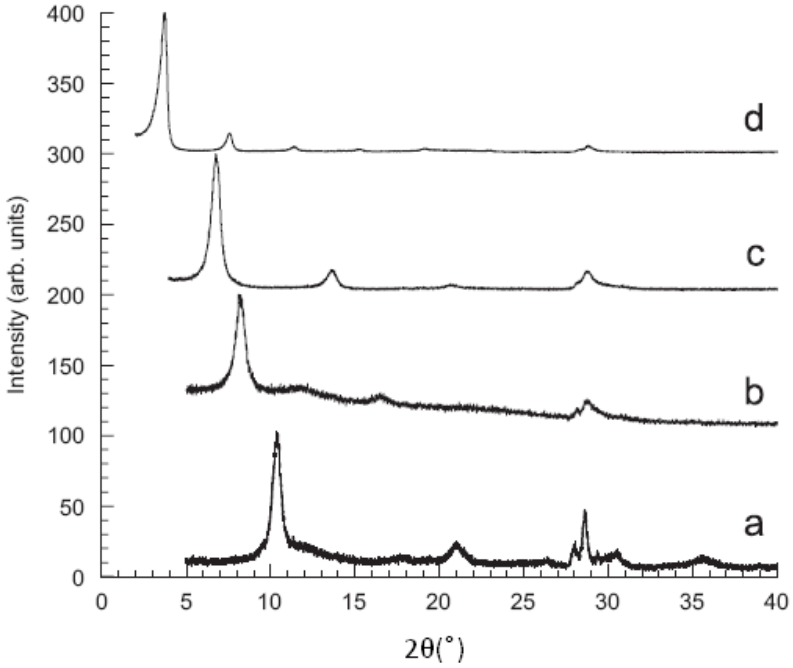

Figure 6 Powder XRD diffraction patterns of:

(a) $Y_2(OH)_5NO_3{\cdot}H_2O$ and the anion exchange intercalation compounds

(b) $Y_2(OH)_5(trans\text{-}C_4H_2O_4)_{0.5}{\cdot}H_2O$,

(c) $Y_2(OH)_5(p\text{-}C_8H_4O_4)_{0.5}{\cdot}H_2O$ and

(d) $Y_2(OH)_5(C_{10}H_{21}SO_4)\ H_2O$.

The data demonstrates the flexibility of these materials as anion exchange intercalation hosts, with interlayer separation increasing three-fold up to 24.5 Å. Comparing the analogous intercalates from the $Ln_2(OH)_5NO_3{\cdot}1.5H_2O$ series it is found that the aromatic anions give similar basal spacings, whilst those for the aliphatics are higher, inferring that these anions are oriented more perpendicularly.

Further evidence of successful reactions is provided by FTIR. Figure 7 shows the FTIR spectrum of $Y_2(OH)_5(p\text{-}C_8H_4O_4)_{0.5}{\cdot}H_2O$ with bands due to the carbonyl stretch of uncoordinated terephthalate anions (1550 and 1390 cm^{-1}) and a broad O-H stretch at approximately 3550 cm^{-1} corresponding to the stretching vibrations of the layer hydroxy groups and the interlayer water molecules. Additionally, the absence of a broad band at 1370 cm^{-1} indicates complete exchange of the uncoordinated interlayer nitrate.

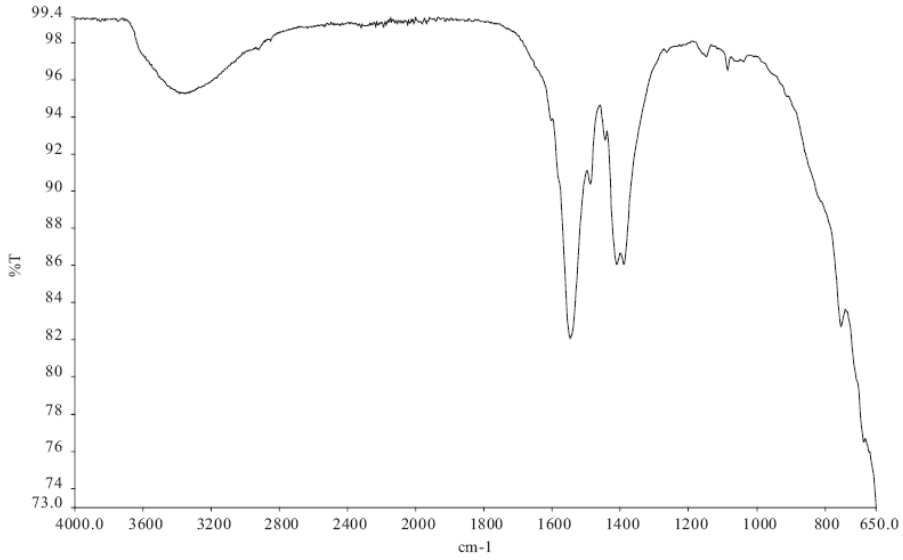

Figure 7 FTIR specrum of $Y_2(OH)_5(p\text{-}C_8H_4O_4)_{0.5}\cdot H_2O$

TGA of these intercalation compounds are similar to that of comparable organic derivatives of LDHs and those described in Chapter 2 and support the assertion that the layer stoichiometry does not change during the reaction. In general decomposition occurs via three distinct mass losses, firstly loss of co-intercalated water, dehydroxylation of the layers and finally decomposition of the organic guest. The TGA trace for $Y_2(OH)_5(p\text{-}C_8H_4O_4)_{0.5}\cdot H_2O$, shown in Figure 8 shows a mass loss of 43.8 %, the calculated mass loss for the material is 41.0 %.

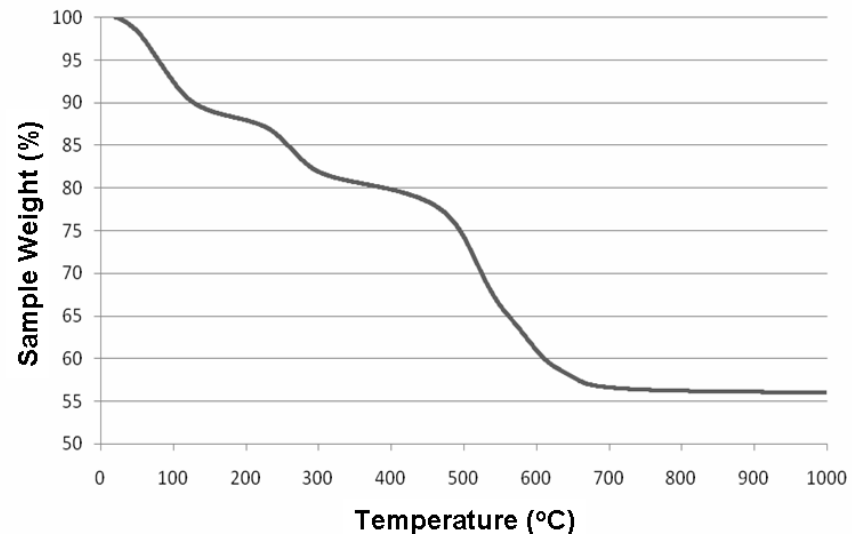

Figure 8 TGA trace for $Y_2(OH)_5(p\text{-}C_8H_4O_4)_{0.5}\cdot H_2O$ showing a total mass loss of 43.8 %.

In this section, the synthesis and anion exchange chemistry of layered lanthanide hydroxynitrate intercalation hosts ($Ln_2(OH)_5NO_3{\cdot}H_2O$, Ln = Eu-Er, Y) has been described. The materials are prepared via a room temperature precipitation method and include the first $Eu_2(OH)_5NO_3{\cdot}H_2O$ host lattice. Anion exchange reactions proceed at room temperature with a range of organic carboxylates and sulfonates. The materials are remarkably flexible with interlayer separations increasing from 8.45 Å to 24.30 Å in the case of $Y_2(OH)_5(C_{10}H_{21}SO_4){\cdot}H_2O$.

4.3 Synthesis and Characterisation of LDHs Containing Precious Metals

4.3.1 Results and Discussion

Attempts to synthesise "layered precious metal hydroxides" containing only Pd or Ru through hydrothermal synthesis following the method described in Chapter 2 for the $Ln_2(OH)_5NO_3{\cdot}1.5H_2O$ materials proved unsuccessful. In a typical reaction an aqueous solution of $Ru(X)_3{\cdot}xH_2O$ or $Pd(X)_2{\cdot}xH_2O$ (X = NO_3, Cl) was added to an aqueous solution containing NaOH and NaX (X = NO_3, Cl) and treated hydrothermally at 150 ºC for 48 hours. Systematic reaction condition screening across metal concentrations (0.1 - 0.45 M), reaction temperatures (100 - 150 ºC) and times (24 - 48 hours) yielded only the corresponding oxides.

It is thought that Ru^{3+} does not form this phase due to the small cation size (0.67 Å), the smaller lanthanide cations (Gd – Lu) are in the range 0.94 – 0.85 Å. Whilst Pd^{2+} is of comparable cation size (0.86 Å) its preferential coordination is square planar. Preferential coordination has been cited by Basile *et al*. as more important than size through an investigation of noble metal containing layered hydroxides.[12] In the study Rh^{3+}, Ru^{3+}, Ir^{3+}, Pd^{2+} and Pt^{2+} MgAl-LDHs materials were obtained, despite the preferential square-planar coordination of Pd^{2+} and palladium cationic radius being at the limit for incorporation into LDHs. However 20 % Pt^{2+} was lost during synthesis whereas Pd^{2+} was incorporated successfully into the lattice.

Attempts were also made to synthesise the layered hydroxides via room-temperature slow-growth and a vapour diffusion method as described by Du and O'Hare.[20] In this method, dilute aqueous solutions of NH_4OH and $RuCl_3{\cdot}xH_2O$ or $PdX_2{\cdot}xH_2O$ (X = NO_3, Cl, OAc) were stored at room temperature for a period of 10 days under reduced pressure. However both methods were unsuccessful, yielding only amorphous materials.

As attempts to synthesise layered hydroxides containing only Pd or Ru were unsuccessful, attention was turned to the doping of these metals into existing LDHs. Initial synthesis routes followed a preparation described for the synthesis of Ni^{2+} - Fe^{3+} LDH,[21] in this way it was envisaged that a Pd^{2+} - Al^{3+} and a Mg^{2+} - Ru^{3+} LDH could be produced. This synthesis, using urea as a hydrolysis agent proved unsuccessful, however room temperature coprecipitation synthesis was subsequently performed following the preparation outlined by Rousselot *et al.* for the synthesis of Ga/Al-containing layered double hydroxides.[22] Typically, syntheses were carried out at 60 ºC with stirring during the dropwise addition of solutions of the metal ions in order to maintain pH 10. Once addition was complete, the resulting suspension was stirred for 24 hours at 60 ºC and the solid product subsequently isolated by repeated centrifugation and washing with water. The solid was then dried in an open air oven at 60 ºC. Preliminary characterisation of the materials prepared is suggestive of Ru having been incorporated into the host lattice of MgAl LDH at higher levels than previously reported.

4.3.1.1 Ruthenium containing MgAl-NO_3 LDHs

In the first instance, the synthesis of Mg_3-Al-NO_3 LDH was carried out to ensure repeatability of the method. Material with the composition $[Mg_{0.72}Al_{0.28}(OH)_2](CO_3)_{0.06}(NO_3)_{0.16}{\cdot}0.63H_2O$ was afforded by following the method described by Rousselot *et al.*[22] Powder X-ray diffraction data, shown in Figure 9, gives an interlayer spacing for the material of 8.40 Å.

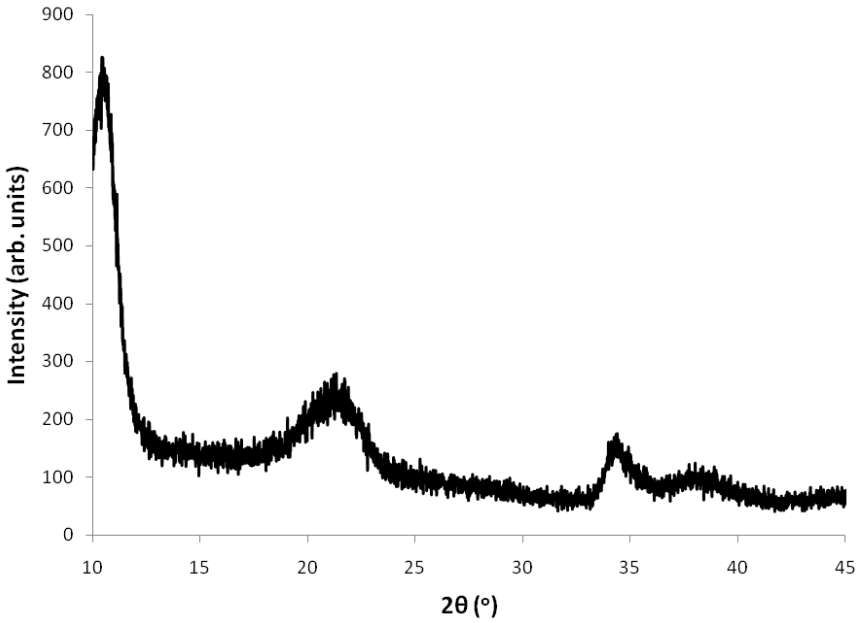

Figure 9 Powder X-ray diffraction pattern of MgAl-NO_3LDH.

Elemental analysis supports the suggested composition, calculated: Mg, 20.83 % Al, 8.99 % H, 3.91 % N, 2.67 % C, 0.86 %. Observed: Mg: 20.42 %, Al: 8.66 %, H: 3.68 %, N: 3.33 %, C: 0.26 %. It is noteworthy that although neither decarbonated water nor a protective nitrogen atmosphere were used, there is lower carbonate contamination observed compared with that previously reported. TGA data shown in Figure 10 shows a total mass loss of 47.7 % to give MgO and Al_2O_3, compared with a calculated value of 48.4 %.

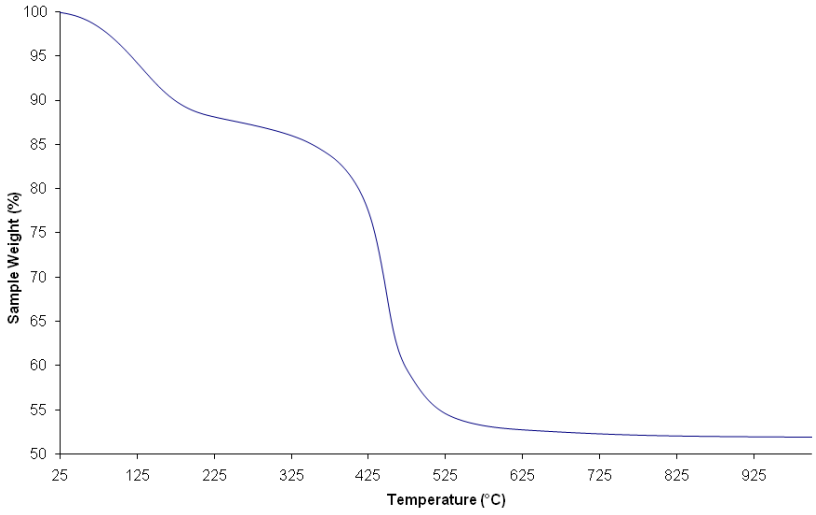

Figure 10 TGA trace for MgAl-NO_3 LDH showing a mass loss of 11.2 % below 200 ºC and a further mass loss of 36.5 % by 700 ºC.

Further confirmation of the Mg:Al ratio can be gathered from Energy dispersive X-ray spectroscopy (EDS). EDS analysis, as shown in Figure 11, confirmed a homogeneous dispersion of Mg^{2+} and Al^{3+} through the host lattice at levels of 78 % and 22 % respectively.

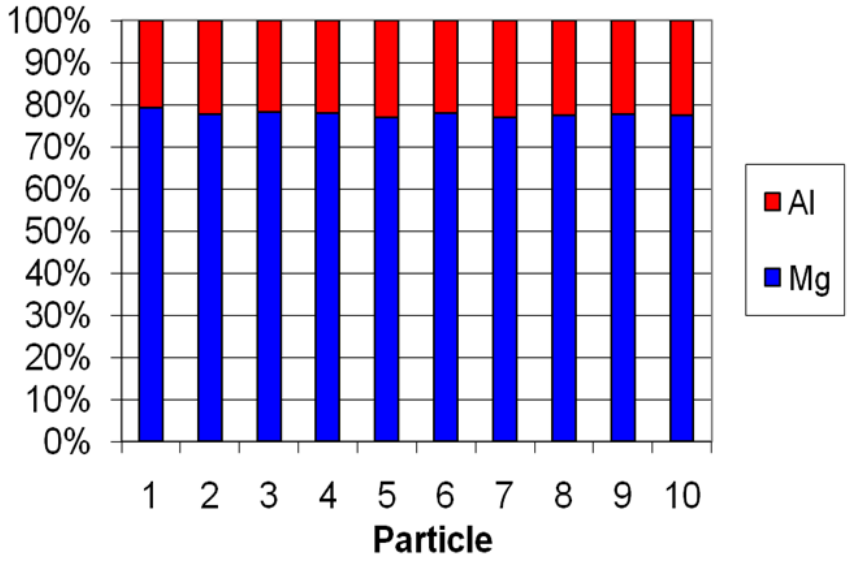

Figure 11 Chart displaying EDS results indicating an average dispersion of Mg: 78 % and Al: 22 % across particles measured.

Having confirmed that the coprecipitation method was repeatable in non-CO_2 free conditions, it was decided that Ru doping in to the Mg_3-Al-NO_3 LDH would be attempted.

The characterising data for MgAlRu-NO_3 and MgRu-NO_3 phases with the target compositions $[Mg_{0.75}Al_{0.11}Ru_{0.14}(OH)_2](CO_3)_{0.04}(NO_3)_{0.16}\cdot 0.54H_2O$ and $[Mg_{0.81}Al_{0.19}(OH)_2](CO_3)_{0.03}(NO_3)_{0.12}\cdot 0.62H_2O$, are summarized in Table 3.

Table 3 Characterising data for the Ru-doped MgAl-NO_3 LDH materials.

Target composition	Interlayer spacing (Å)	Elemental Analysis	
		Observed (%)	Calculated (%)
$[Mg_{0.75}Al_{0.11}Ru_{0.14}(OH)_2](CO_3)_{0.04}(NO_3)_{0.16}\cdot 0.54H_2O$	8.09	Mg (19.02)	Mg (19.94)
		Ru (14.99)	Ru (15.48)
		Al (3.66)	Al (3.25)
		H (3.65)	H (3.40)
		N (1.54)	N (2.45)
		C (0.38)	C (0.53)
$[Mg_{0.81}Ru_{0.19}(OH)_2](CO_3)_{0.03}(NO_3)_{0.12}\cdot 0.62H_2O$	7.88	Mg (11.77)	Mg (21.10)
		Ru (19.45)	Ru (20.58)
		H (3.38)	H (3.50)
		N (1.29)	N (1.80)
		C (0.49)	C (0. 39)

Notably, in the case of MgAlRu-NO_3 material, the Mg / (Al + Ru) molar ratio is different from that used in the starting solutions, at approximately half of that expected.

Powder X-ray diffraction data for the phases is shown in Figure 12. The MgAlRu-NO_3 material (Figure 12a) is phase pure, with 00*l* reflections indicative of a lamellar phase, with an interlayer spacing of 8.09 Å. The MgRu-NO_3 material however, is completely amorphous (Figure 12b).

TGA data for the phases are shown in Figure 13, with full decomposition to MgO, RuO_2 (and Al_2O_3) by 500 ºC. MgAlRu-NO_3 LDH displays a total mass loss of 43.9 % (calculated 40.5 %) and MgRu-NO_3 LDH shows a total mass loss of 38.5 % (calculated 38.0 %).

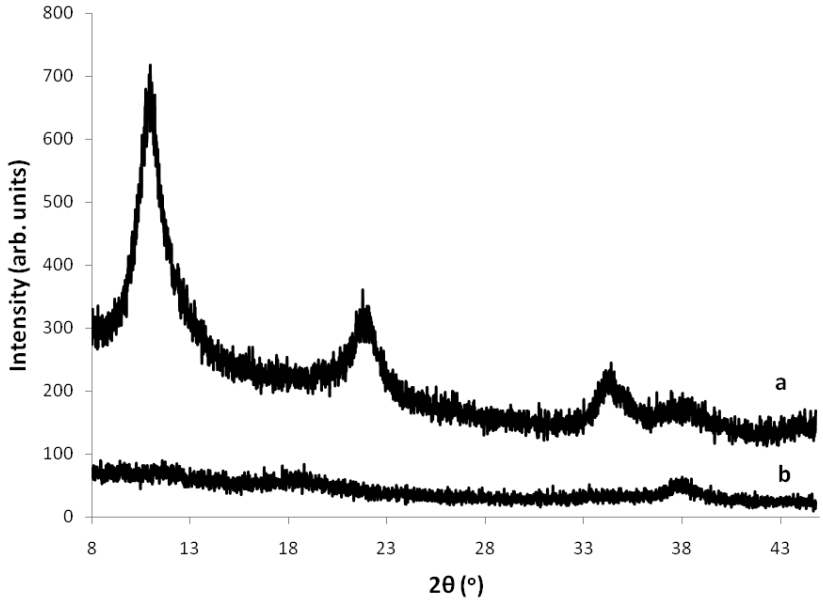

Figure 12 Powder X-ray diffraction pattern of:

(a) MgAlRu-NO_3 LDH and

(b) MgRu-NO_3 LDH.

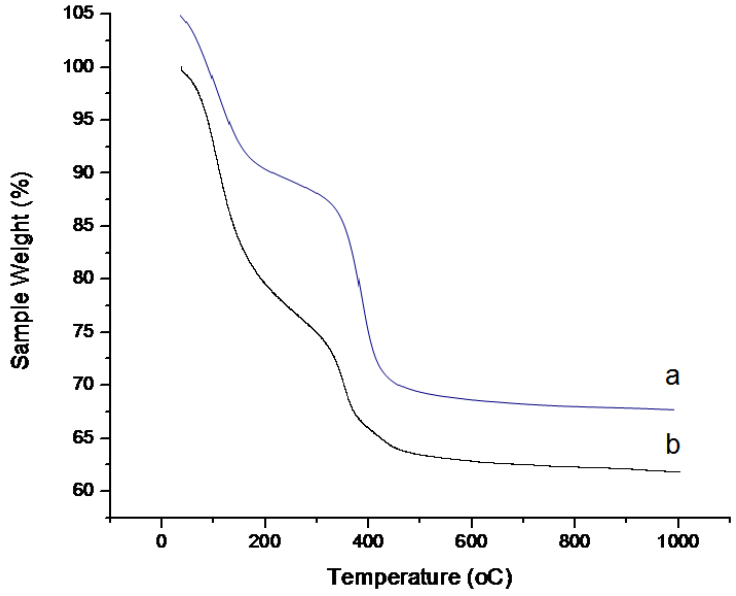

Figure 13TGAs traces for;

(a) MgAlRu-NO_3 LDH (showing a mass loss of 43.9 %) and

(b) MgRu-NO_3 LDH (showing total mass loss of 38.5 %).

NB. Top trace is shifted upwards by an arbitrary 5 % to allow comparison between the two phases.

EDS analysis confirms an appropriate dispersion of metal cations across the sample. EDS for MgAlRu-NO_3 LDH as shown in Figure 14a, confirms a Mg:Al:Ru ratio of 77:11:14. MgRu-NO_3 analysis confirms a ratio of 79:21 (Figure 14b). These values are consistent with the metal ratios provided by bulk ICP analysis.

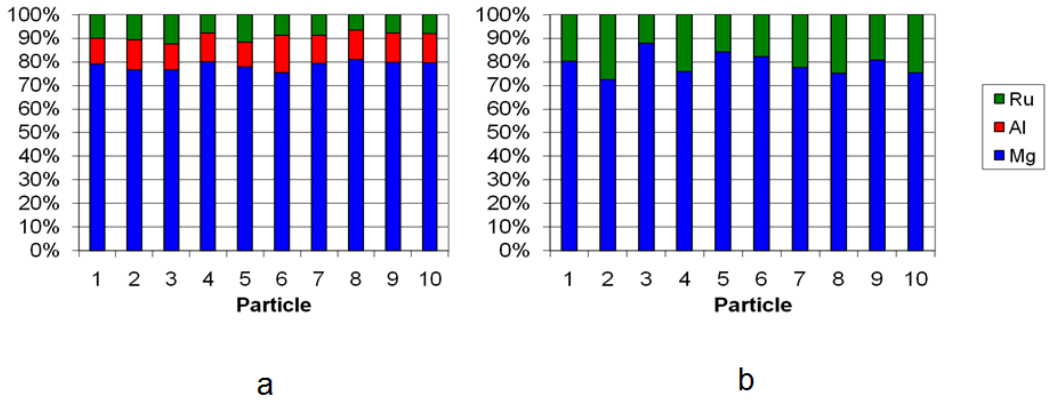

Figure 14 Chart to display EDS results for:

(a) MgAlRu-NO_3 LDH indicating average values of Mg: 77 %, Al: 11 %, Ru: 14 % and

(b) MgRu-NO_3 LDH indicating average values of Mg: 79 %, Ru: 21 % across the particles measured.

To further characterise the MgAlRu-NO_3 material, SEM imaging was carried out (Figure 15). Consistent with PXRD data, the morphology of this material is less crystalline than the well-defined hexagonal plate morphology of the layered hydroxides described in Chapter 2 (Chapter 2, Figure 6). Whilst some crystallites have a characteristic plate structure, the material is not homogeneous, suggesting the presence of some amorphous phases.

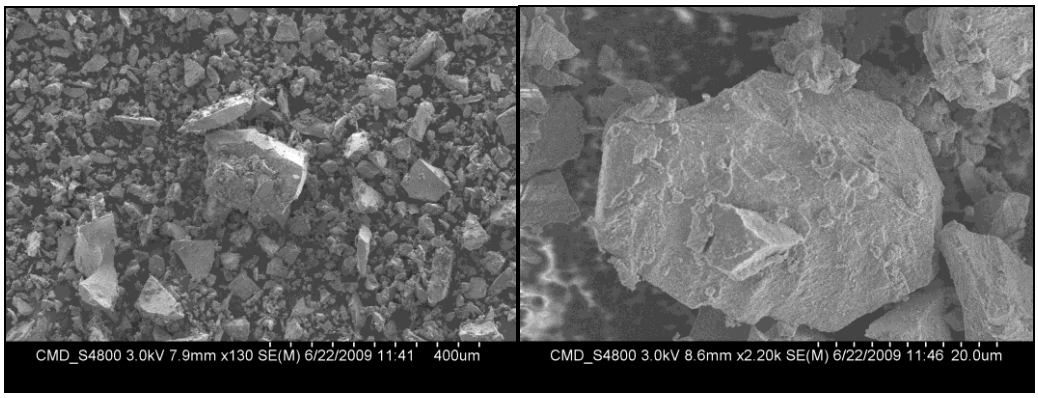

Figure 15 SEM images showing unusual morphology of MgAlRu-NO_3 material (SEM by G. Evans).

Room temperature anion exchange reactions of the MgAlRu-NO_3 material were attempted with sodium terepththalate, to ascertain whether the interlayer nitrate anions were exchangeable. This reaction proved unsuccessful, suggesting possible coordination of the anion to the metal cations. The FTIR spectrum of MgAlRu-NO_3 is shown in Figure 16. The key features of the spectrum are a broad absorption at approximately 3400 cm^{-1} corresponding to a combination of the stretching vibrations of the layer hydroxyl groups and the interlayer water molecules and the bending vibration of water at 1640 cm^{-1}. The band at 1340 cm^{-1} may indicate the presence of nitrate, however it is also known that the v_3 mode of CO_3^{2-} appears in this region.[23] A small band at 1050 cm^{-1} (ν_1 mode resulting from reduced symmetry of the intercalate) and 1760 cm^{-1} (combination mode typical of nitrate) confirm the presence of nitrate. There is no evidence of splitting in the region 1300 – 1450 cm^{-1} indicating that the nitrate is not coordinated to the metal layer.[15] Additional reaction screening is required to ascertain the anion exchange capacity of these materials, including a wider range of anions and reaction temperatures.

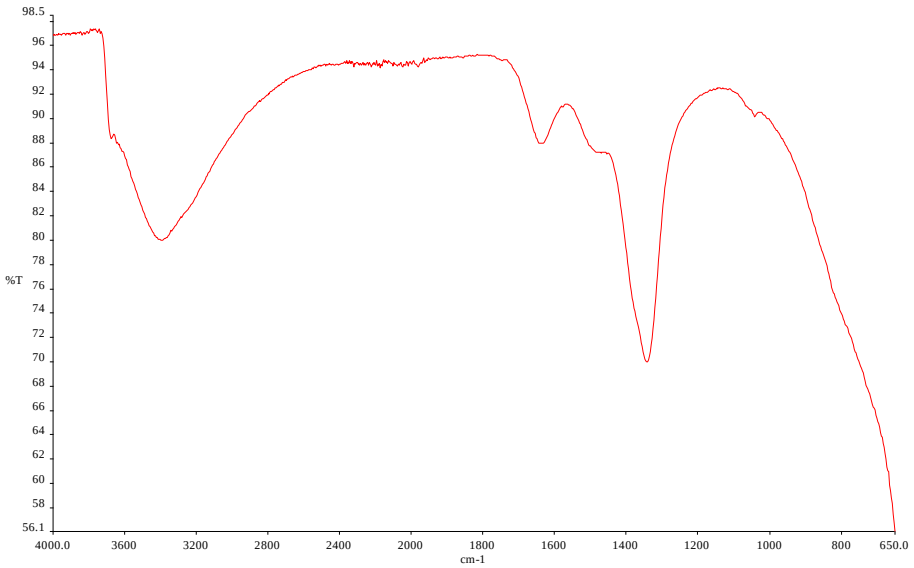

Figure 16 FTIR spectra for MgAlRu-NO_3 LDH material.

4.3.1.2 Ruthenium containing MgAl-Cl LDHs

Ru-doped MgAl LDHs with interlayer chloride were prepared with M^{2+} / M^{3+} ratio of 3 and Ru / (Al + Ru) ratios of 0.5 and 1. MgAlRu-Cl was synthesised via the

dropwise addition of an aqueous solution of $MgCl_2 \cdot xH_2O$, $AlCl_3 \cdot xH_2O$ and $RuCl_3 \cdot xH_2O$ and a NaOH solution to water, maintaining the pH at 10. Once addition was complete, the solution was aged at 60 ºC for 24 hours. The synthesis of MgRu-Cl was also achieved following this method, with the omission of $AlCl_3 \cdot xH_2O$.

The characterising data for MgAlRu-Cl and MgRu-Cl phases with the target compositions $[Mg_{0.75}Al_{0.11}Ru_{0.14}(OH)_2](CO_3)_{0.04}(Cl)_{0.16} \cdot 0.54H_2O$ and $[Mg_{0.81}Al_{0.19}(OH)_2](CO_3)_{0.03}(Cl)_{0.12} \cdot 0.62H_2O$, are summarized in Table 4.

Table 4 Characterising data for the Ru-doped MgAl-Cl LDH materials.

Target composition	Interlayer spacing (Å)	Elemental Analysis	
		Observed (%)	Calculated (%)
$[Mg_{0.75}Al_{0.11}Ru_{0.14}(OH)_2](CO_3)_{0.04}(Cl)_{0.16} \cdot 0.54H_2O$	8.09	Mg (12.67)	Mg (20.67)
		Ru (9.80)	Ru (16.41)
		Al (1.59)	Al (3.41)
		H (3.79)	H (3.57)
		C (0.34)	C (0.55)
$[Mg_{0.81}Ru_{0.19}(OH)_2](CO_3)_{0.03}(Cl)_{0.12} \cdot 0.62H_2O$	7.88	Mg (12.40)	Mg (21.84)
		Ru (19.53)	Ru (21.31)
		H (2.98)	H (3.62)
		C (0. 90)	C (0.40)

Notably, the Mg / (Al + Ru) molar ratios are different from those used in the starting solutions, this disparity in metal ratios was also observed by Rousselot *et al*. As for the nitrate materials described in section 4.3.1.1 Mg levels are approximately 50 % lower than that used in the starting solutions. Additionally, in the case of MgAlRu-Cl, Ru and Al content is also lower than expected.

Powder X-ray diffraction data for the phases is shown in Figure 17. The materials are phase pure and display 00*l* reflections characteristic of layered materials, with d-spacings of ~ 8.0 Å. MgAlRu-Cl LDH (Figure 17a) is noticeably more crystalline than MgRu-Cl LDH (Figure 17). The baselines for the patterns are not level, as observed in other Ru containing systems.[10] Both the MgRu-Cl and MgRu-NO_3 materials are less crystalline than the analogous Al containing materials, which suggests that Al^{3+} is required in the host lattice to form the Ru-containing phases.

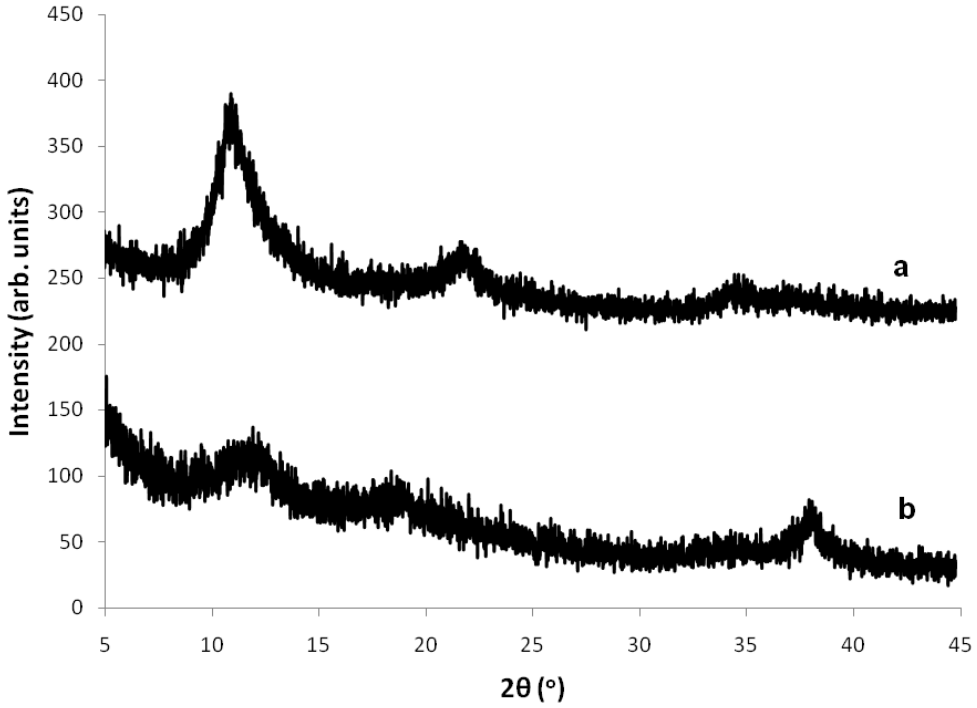

Figure 17 Powder X-ray diffraction patterns of;

(a) MgAlRu-Cl LDH and

(b) MgRu-Cl LDH.

TGA data for the phases is shown in Figure 18, with full decomposition to MgO, RuO_2 (and Al_2O_3) by 500 ºC. MgAlRu-Cl LDH displays a total mass loss of 42.2 % (calculated 37.6 %) and MgRu-Cl LDH shows a total mass loss of 37.0 % (calculated 35.8 %).

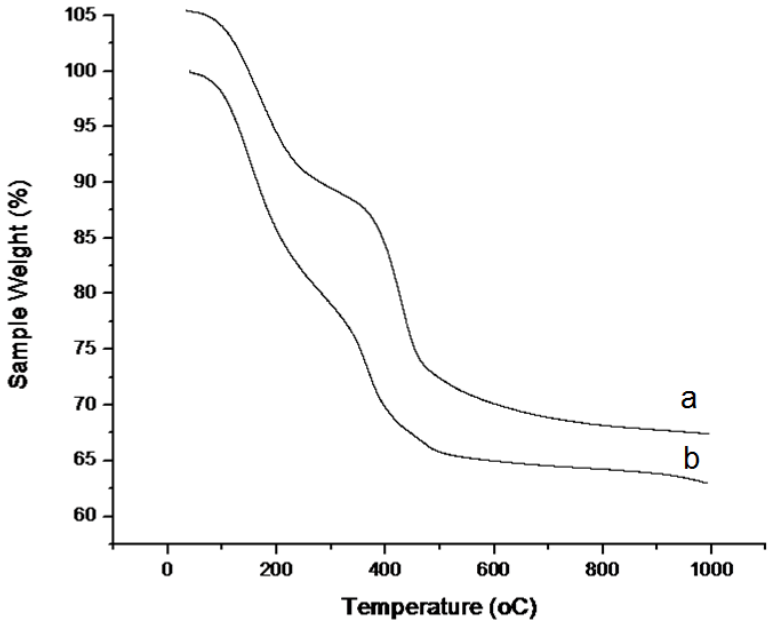

Figure 18 TGAs traces for;

(a) MgAlRu-Cl LDH (showing a mass loss of 42.2 %) and

(b) MgRu-Cl LDH (showing a mass loss of 37.0 %).

NB. Top trace is shifted upwards by an arbitrary 5% to allow comparison between the two phases.

4.4 Summary

The synthesis and anion exchange chemistry of layered lanthanide hydroxynitrate intercalation hosts ($Ln_2(OH)_5NO_3{\cdot}H_2O$, Ln = Eu-Er, Y) has been described. The materials are prepared via a room temperature precipitation method and include the first $Eu_2(OH)_5NO_3{\cdot}H_2O$ host lattice. Anion exchange reactions proceed at room temperature with a range of organic carboxylates and sulfonates. The materials are remarkably flexible with interlayer separations increasing from 8.45 Å to 24.30 Å in the case of $Y_2(OH)_5(C_{10}H_{21}SO_4){\cdot}H_2O$.

Since the publication of the precipitation synthesis of $Ln_2(OH)_5NO_3{\cdot}H_2O$ (Ln = Eu-Er, Y), the homogeneous precipitation synthesis routes to $Gd(OH)_{2.5}Cl_{0.5}{\cdot}0.9H_2O$:0.05Eu solid solutions and $Ln_8(OH)_{20}(NO_3)_{4\ 3}{\cdot}nH_2O$ (Ln = Sm-Tm, Y) have been outlined by Sasaki *et al*.[24,25]

In the second part of this chapter, the feasibility of incorporating precious metals Ru and Pd into layered hydroxides was investigated. Hydrothermal, vapour diffusion and coprecipitation methods were examined. Synthesis by methods other than precipitation were found to be unsuccessful. Materials were synthesised by coprecipitation and characterisation suggests that Ru has been incorporated into layered hydroxides at levels of up to 20 %.

PXRD confirms that MgAlRu-NO_3, MgAlRu-Cl and MgRu-Cl materials are lamellar and phase pure, with interlayer spacings of ~ 8. 0 Å. Further SEM characterisation of MgAlRu-NO_3 reveals plate morphology typical of layered hydroxides, however the non-homogeneous morphology suggests that there is some amorphous material present. EDS and bulk ICP analysis for this material confirms doping of Ru at levels of 14 %. ICP analysis of MgAlRu-Cl and MgRu-Cl suggests doping at levels of 10 and 20 % respectively.

Further characterisation of these materials is required; however, these preliminary results are indicative of a lamellar phase incorporating Ru into the MgAl LDH host lattice at levels of up to 20 %. This is higher than levels previously reported of 7 % for Ru-doped CoAl-LDH.[9]

4.5 References

1. F. X. Geng, Y. Matsushita, R. Z. Ma, H. Xin, M. Tanaka, F. Izumi, N. Iyi and T. Sasaki, *Journal of the American Chemical Society*, 2008, **130**, 16344-16350.
2. F. X. Geng, H. Xin, Y. Matsushita, R. Z. Ma, M. Tanaka, F. Izumi, N. Iyi and T. Sasaki, *Chemistry-a European Journal*, 2008, **14**, 9255-9260.
3. M. Komiyama, *Catalysis Reviews-Science and Engineering*, 1985, **27**, 341-372.

4. E. P. Giannelis, D. G. Nocera and T. J. Pinnavaia, *Inorganic Chemistry*, 1987, **26**, 203-205.
5. J. Inacio, C. Taviot-Gueho, S. Morlat-Therias, M. E. d. Roy and J. P. Besse, *Journal of Materials Chemistry*, 2001, **11**, 640-643.
6. F. A. Khan and N. Sahu, *Journal of Catalysis*, 2005, 438-442.
7. F. Cavani, F. Trifiro and A. Vaccari, *Catalysis Today*, 1991, **11**, 173-301.
8. K. Kaneda, T. Yamashita, T. Matsushita and K. Ebitani, *Journal of Organic Chemistry*, 1998, **63**, 1750-1751.
9. T. Matsushita, K. Ebitani and K. Kaneda, *Chemical Communications*, 1999, 265-266.
10. F. Basile, L. Basini, G. Fornasari, M. Gazzano, F. Trifiro and A. Vaccari, *Chemical Communications*, 1996, 2435-2436.
11. F. Basile, G. Fornasari, V. Rosetti, F. Trifiro and A. Vaccari, *Catalysis Today*, 2004, 293-297.
12. F. Basile, G. Fornasari, M. Gazzano and A. Vaccari, *Applied Clay Science*, 2000, **16**, 185-200.
13. A. V. Besserguenev, A. M. Fogg, R. J. Francis, S. J. Price, D. O'Hare, V. P. Isupov and B. P. Tolochko, *Chemistry of Materials*, 1997, **9**, 241.
14. S. Miyata, *Clays and Clay Minerals*, 1983, **31**, 305-311.
15. S. P. Newman and W. Jones, *Journal of Solid State Chemistry*, 1999, **148**, 26-40.
16. I. Schildermans, J. Mullens, J. Yperman, D. Franco and L. C. Vanpoucke, *Thermochimica Acta*, 1994, **231**, 185-192.
17. J. M. Haschke, *Inorganic Chemistry*, 1974, **13**, 1812-1818.
18. G. W. Beall, *Journal of Inorganic & Nuclear Chemistry*, 1977, **39**, 65-&.
19. A. M. Fogg, G. R. Williams, R. Chester and D. O'Hare, *Journal of Materials Chemistry*, 2004, **14**, 2369-2371.
20. Y. Du and D. O'Hare, *Journal of Physics and Chemistry of Solids*, 2008, **69**, 1040-1043.
21. Y. Han, Z. Liu, Z. Yang, Z. Wang, X. Tang, T. Wang, L. Fan and K. Ooi, *Chemistry of Materials*, 2008, **20**, 360-363.
22. I. Rousselot, C. Taviot-Gueho and J. P. Besse, *International Journal of Inorganic Materials*, 1999, **1**, 165-174.

23. J. T. Kloprogge, L. Hickey and R. L. Frost, *Journal of Raman Spectroscopy*, 2004, **35**, 967-974.
24. L. F. Hu, R. Z. Ma, T. C. Ozawa and T. Sasaki, *Angewandte Chemie-International Edition*, 2009, **48**, 3846-3849.
25. F. X. Geng, Y. Matsushita, R. Z. Ma, H. Xin, M. Tanaka, N. Iyi and T. Sasaki, *Inorganic Chemistry*, 2009, **48**, 6724-6730.